Thin–Walled Structures 195 (2024) 111364

Contents lists available at ScienceDirect

Thin-Walled Structures

journal homepage: www.elsevier.com/locate/tws

Full length article

Experimental characterization and modeling of cylindrical CFRP structures under quasi-static multiaxial loading conditions

Szymon Duda [a,*], Michał Smolnicki [a], Paweł Stabla [a], Paweł Zielonka [a], Tomasz Osiecki [b], Chao Gao [c], Grzegorz Lesiuk [a]

[a] Faculty of Mechanical Engineering, Wroclaw University of Science and Technology, Wroclaw, Poland
[b] Polymer-based Lightweight Design, Brandenburg University of Technology, Cottbus, Germany
[c] Department of Mechanical and Industrial Engineering, Norwegian University of Science and Technology, Trondheim, Norway

ARTICLE INFO

Keywords:
CFRP
Nonlinear shear behavior
FEA
Experimental mechanics

ABSTRACT

An experimental and numerical investigation of the cylindrical carbon fiber reinforced polymer (CFRP) structures under various loads including tension/torsion loading conditions has been conducted. Various boundary conditions and parameters were taken into account to check the impact of the shear component to obtain the result. The nonlinear shear model proposed by Chang has been implemented to take into account the softening effect of the stress-strain curve caused by damage accumulation. The computational model of the thin-walled tubes contains the geometrical architecture of the material, such as interweaving, which are characteristic of the parts made by filament winding technology. The studies were preceded by preliminary tests of the individual components to predict elastic properties based on the Abolin'sh micromechanical approach. The strength parameters were empirically delivered on the basis of the experimental results and used to determine the failure of the structure. The accuracy of the calibrated nonlinear shear model was validated using strain gauges and digital image correlation techniques. The strain distribution obtained from FEA was compared with that of the optical method. The damage distribution provided by FEA is exhibited in a similar manner to the real one captured by DIC. The proposed model provides a precise prediction of the CFRP tubes under quasi-static loading conditions proven by the experiments.

List of abbreviations

λ_t	biaxiality ratio
α	nonlinearity factor
CFRP	carbon fiber reinforced polymer
DIC	digital image correlation
e_m	matrix tensile/compressive failure criterion
e_{fs}	fiber—matrix shearing criterion
e_b	fiber buckling criterion
E_1	Young modulus along fibers (1st-direction)
E_2	Young modulus perpendicular to fibers
FEM/A	Finite Element Method/Analysis
FV	Field Variable
FW	filament winding
G_{ij}	Shear modulus in "ij" direction
ν_{ij}	Poisson ratio in "ij" direction
S_c	ply shear strength
$\sigma_{ij,a}$	shear stress component
$\sigma_{i,a}$	normal stress component
PS	principal strain
UTS	Ultimate Tensile Strength
X_c	longitudinal compressive strength
γ_{ij}	shear strain in "ij" direction
Y_c	matrix compressive strength
Y_t	transverse tensile strength
WP	winding pattern

1. Introduction

The remarkable mechanical performance of composite materials is very attractive for structural engineering; however, a difficult design process remains a major barrier to the wider application of composite

* Corresponding author.
E-mail address: szymon.duda@pwr.edu.pl (S. Duda).

https://doi.org/10.1016/j.tws.2023.111364
Received 25 July 2023; Received in revised form 19 September 2023; Accepted 10 November 2023
Available online 11 November 2023

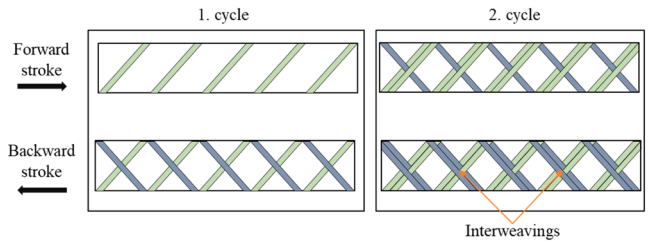

Fig. 1. Schematic presentation of filament winding processes in the example of two cycles.

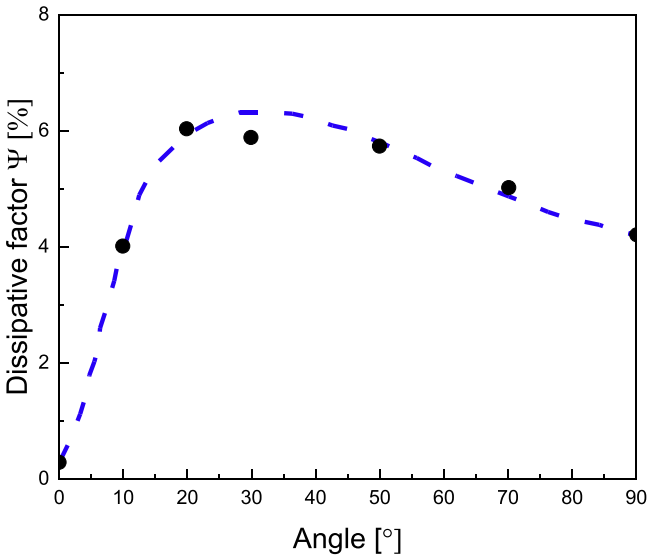

Fig. 2. Calculated (dot line) and experimental (black points) dependencies of dissipation factor on the ply orientation for carbon epoxy unidirectional composites adapted from [7].

materials. The difficulty comes from the multiaxial stress states caused by the anisotropy of the material. In reality, this stress state can also be compounded by multiaxial cyclic loading conditions. To overcome these difficulties, the computer-aided method, which allows the numerical delivery of the constitutive relationship, has been exploited in recent decades and has been demonstrated to be an effective approach. However, a comprehensive experimental investigation is mandatory to calibrate the material model and then verify the stress-strain behavior predicted by numerical simulations.

There are only a few significant research groups in the world that deal with the multiaxial behavior of composite materials [1–3]. It is mainly due to the demanding specification of the research. The experiment under multiaxial loading conditions (e.g. tension/torsion) is time-consuming and cost-consuming as well as requires special apparatus (biaxial servohydraulic testing system) in wake of that, not every research team can afford this.

Assumed loading conditions of tension, compression, and torsion appear in many industrial applications such as wings or turbine blades. They are subjected to aerodynamic loads that induce bending (i.e. tension and compression) coupled with torsion (shear); the investigation of such a state is well justified and not yet fully described [4]. When these loading conditions are established, the appropriate specimen should be manufactured. Olsson [5] submitted a review article giving an overview of multiaxial test methods, suggesting that a tubular specimen is an obvious choice for these assumptions (material and loading conditions). Moreover, this type of specimen shows the absence of a free edge effect. There are two possibilities for making this type of sample using the filament winding or mandrel wrapping and curing process in an autoclave [6].

The presented research concerns the mechanical performance of tubular thin-walled carbon fiber reinforced polymer (CFRP) under basic loading conditions, as well as under multiaxial loading conditions. Due to the highly complex stress state in composite material under multiaxial external loads, Quaresimin [6] has proposed an additional parameter such as the biaxiality ratio, which describes the degree of multiaxiality of the stress state. In this research, the biaxiality ratio of the geometrical stresses is taken into account and is assumed to be as follows.

a *The biaxiality ratio*, denoted T, is a ratio of the geometric stress components as follows:

$$\lambda_T = \frac{\tau_{xy}}{\sigma_x} \tag{1}$$

where τ_{xy} is a shear component, and σ_x is a stress component along the applied axial force.

Manufacturing composite structures using the filament winding method leads to a specific fiber distribution and orientation. The process itself is cyclic, where the composite layer is wound on the mandrel with a band of roving fiber. The bandwidth determines the number of cycles necessary to cover the circumference of the mandrel. In one cycle, the forward and backward strokes are determined. The first stroke is wound with the positive winding angle and the backward stroke is wound with the negative angle. The second cycle is wound next to the previous one (this depends on the mosaic pattern) and in some areas, the impregnated fibers cover the previous ones (Fig. 1).

The effect of the cyclic process of filament winding technology is the specific structure of the composite with interweavings. Interweavings are an inevitable part of the filament wound structure (apart from pure hoop winding). In this area, the fibers are distorted from the linear path and may be the cause of stress concentration.

Fiber orientation is an important parameter that needs to be defined while FW tubes are manufactured. There are many factors that can be taken into account. The main factor depends on the applicability and the forces that act on the composite part. In the case of this research, the fiber orientation was chosen at 30°. This assumption was made based on the dissipative factor and the calculations provided by Morozov [7]. The dependence of the dissipative factor on the fiber orientation is presented in Fig. 2.

Filament wound cylinders are objects of interest to many researchers. Significant effort is put into describing the influence of the winding pattern. Recently, de Menezes et al. [8] investigated the effect of the winding pattern on filament-wound cylinders under axial compression, torsion, and internal pressure loads. The authors developed an original approach to generate the geometric pattern and analyze parameters such as the winding pattern, the number of layers, and the winding angles using the finite element method. The numerical results obtained show that the interweaving regions are the locations of the stress concentrations. Additionally, a very important aspect is placed on the number of layers, which may reduce the effect of the winding pattern. Another scientific paper presented by Lisboa et al. [9] provides an experimental and numerical investigation of the winding pattern. The conclusions drawn show that the winding pattern defines the mechanical response (from yielded progressive to brittle manner) and the manner of failure (delamination, transverse cracks). The authors stated that the stiffness along the patterns did not change significantly; however, the absorbed energy changed between patterns. Original research on the winding pattern is also presented by Azevedo et al. [10]. The influence of mosaic pattern on hygrothermally aged filament wound composite cylinders is well described in the research. The results show that the higher water uptake exhibit pattern 1/1. A lower degree of

Table 1
Mechanical properties of subcomponents used for manufacturing purposes.

Material overview	ZOLTEK™ PX35—continuous carbon fiber experimental data	Araldite LY1564—epoxy resin experimental data
Tensile strength	2422 MPa	49.5 MPa
Young Modulus	230 GPa	2.7 GPa
Elongation	1.42 %	1.8 %
Poisson	–	0.4

interweaving allows greater water uptake. Subsequently, the investigated compressive strength and stiffness were sensitive to the wind pattern. Compressive strength generally increases with the winding pattern; on the other hand, the highest stiffness was obtained for pattern 3/1. It is necessary to refer to the work of Morozov [11], which shows that stress analysis based on the conventional mechanics of laminated structures could underestimate these values. The results state that the mechanical behavior of the thin-walled filament wound composite shells is sensitive to winding patterns, resulting in different stress and strain distributions. At the same time, another study by Morozov [12] should be highlighted, which also shows the importance of the mosaic pattern on the mechanical performance of FW structures. The literature review provides the appropriate direction in terms of stress/strain analysis. Regarding numerical methods and FW structures, it is important to take into account the mosaic pattern, which has a significant impact on the stress distribution.

Consequently, a proper material model with progressive failure is necessary to describe the investigated FW material. In 1987, Chang [13] proposed an analytical solution for damage analysis in laminated composites with a notch subjected to compressive loading. The model incorporates the stress analysis along with a failure analysis. The stresses and strains are calculated on the basis of finite deformation theory with material and geometric nonlinearities. Material failures are predicted on the basis of the set of proposed failure criteria and material degradation models. Good agreement is shown between the predictions and the test results. In 2006, Van Paepegem et al. [14] developed a model with two state variables: shear damage and permanent shear strain. Evolution laws were derived from the experimental data. The author concluded that shear damage can be properly simulated, but the effect of normal stresses cannot be neglected. The author suggested that additional damage laws for transverse stiffness need to be developed. Then in 2012, He et al. [15] developed a method for an accurate assessment of the non-linear shear stress-strain relationship. The presented method combines the finite element method for stress calculation and digital image correlation for full field measurement of deformation. The author incorporated classical beam theory and the Ramberg–Osgood equation into the proposed method to assess the nonlinear shear stress–strain relations of a glass/epoxy tape composite based on short beam shear (SBS) tests. The author stated that the experimentally generated strain field agrees well with the FE-computed strain field. In 2016, Fedulov et al. [16] studied the influence of non-linear plane shear stiffness phenomena on damage and failure. The authors used the stress-strain relation proposed by Chang for the open-hole compression test. The results presented show good agreement with the experiment. Recently, in 2021, O'Brien [17] investigated hybrid composites (glass and steel fibers) as an alternative with increased strength and energy dissipation compared to conventional glass fiber-reinforced composites. The author developed two user-defined material models; first, the material model is based on the continuum damage mechanics that reflect the non-linear behavior of the glass fiber-reinforced epoxy. The second material is based on the plasticity model and reflects the ductile behavior of stainless steel fibers. The proposed method was able to reflect the strain fields captured by the digital image correlation during the experiment. In this study, the model proposed by Chang was chosen among the highlighted approaches due to the boundary conditions assumed in the presented research and the accessibility of use.

On the basis of the literature review, the assumptions for this research were established. The main objective of the research is to characterize the mechanical performance of thin-walled CFRP tubes under various loading conditions. The characterization includes the numerical model to estimate the non-linear shear behavior of the investigated material. The innovative nature of the research is put into two aspects. First, the material and loading conditions, which are not commonly considered. A lot of papers are focused on glass fiber-reinforced polymers under multiaxial conditions, and in this research, a CFRP with 30° degree fiber angle is being considered. Second, the computational method developed for delivering nonlinear stress-strain behavior, including areas with local stress concentration (zigzag), contributes to the detailed design process of composite structures in many industrial sectors.

2. Manufacturing and testing

The description of the chosen material, sample preparation, and testing is presented in this section. The initial phase of the research consisted of testing constituents (single fiber, resin) to estimate elastic properties based on the micromechanical approach. The filament winding method was chosen for the production of the required thin-walled CFRP tubes. Manufactured samples had to be prepared for assumed mechanical testing by providing a stochastic pattern for DIC and positioning the strain gauge rosette. The procedures applied to this research are summarized below.

1) Constituents testing (epoxy resin and single-fiber tensile test),
2) Sample manufacturing and post-curing,
3) Sample preparation for strain measurement (DIC, strain gauge rosette),
4) Mechanical testing.

2.1. Materials and sample preparation

The thin-walled CFRP tubes investigated were manufactured from the following constituents. The reinforcement, PX35 carbon fiber (CF), was purchased from ZOLTEK™. The reinforcement has a diameter of 7.2 μm and a 95 % carbon content. The resin matrix, Araldite LY1564 epoxy resin with Aradur 3474 hardener, was supplied by Huntsman. It was relevant to deliver the mechanical properties of those materials. The elastic properties and UTS were obtained by performing the single fiber tensile test and the dog bone sample for epoxy resin. A single-fiber tensile test was performed on the Textechno FAVIMAT+ machine. This device is equipped with a high resolution load cell (1 μN at 200 cN full range). The results for fiber and epoxy resin are provided in Table 1.

The elastic properties of the constituents allow the application of the micromechanical approach for estimation of the elastic properties of the laminae. The Abolin'sh approach has been applied to predict all ply elastic constants [18]. In this method, ply is assumed to be transversely isotropic in the plane normal to the fibers and neglected the Poisson effect normal to the fibers under longitudinal load. Simultaneously, the elastic properties were compared with those of the Abaqus built-in hexagonal unit cell.

Filament winding technology was applied to manufacture thin-walled tubes of one layer with a mosaic pattern of 1/1. In the process, chrome-coated steel mandrels with a diameter of 20 mm were used. Before each winding process, the mandrel was covered with wax and then polished to facilitate the demolding process. The winding angle was set at 30°. After winding, special shrink tape was applied to the wet surface of the sample to remove the large amount of resin and provide the proper smoothness of the external surface. The composite tubes were then cured at room temperature and in rotation movement. Then, they were demolded from the mandrel, cut into samples, and cured in the

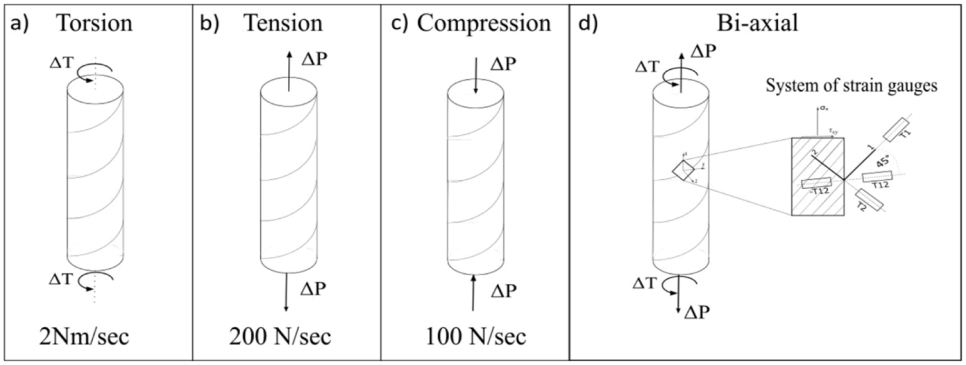

Fig. 3. The conducted loading conditions; a) torsion, b) tension, c) compression, d) biaxial (tension and torsion).

Fig. 4. Experimental setup used in the presented research equipped with a camera I used for sample monitoring, camera II as a part of used DIC system, and strain gauges.

Table 2
Comparison of the elastic properties of the composite with 55 % fiber volume (with the assumption of orthotropic plane stress).

Approach	E_1 [MPa]	E_2 [MPa]	ν_{12} [−]	G_{12} [MPa]
Abolin'sh	128,100	5378	0.345	3132
Hexagonal Unit Cell	128,110	6666	0.343	3145

Table 3
Strength parameters used in the nonlinear shear model.

Transverse tensile strength (Y_t)	Longitudinal compressive strength (X_c)	Transverse compressive strength (Y_c)	Ply shear strength (S_c)
160 MPa	1500 MPa	160 MPa	50 MPa

oven according to the resin producer's recommendations (1 h at 80 °C and 4 h at 120 °C).

The outer diameter of the sample and the orientation of the fiber were measured using the 3D scanning method. Some discrepancy was observed from the orientation of the reference fiber. The standard deviation of the measured angle is 0.45 with respect to the reference angle of 30°. The outer diameter (inner diameter is equal to 20 mm) measured by 3D scanning totals 21.970 mm, with a 0.453 mm discrepancy in circularity. In addition, the diameter was calculated by measuring the length of the sample, the mass and applying the material density (0.00152 g/mm^3). It gives the average value of 21.854 with standard deviation totals of 0.058.

2.2. Methods

The experimental campaign combines various loading conditions applied to the thin-walled CFRP tube with strain gauges and digital image correlation. The samples with stochastic pattern and strain gauge rosette were subjected to several mechanical tests, such as tension, compression, torsion and biaxial, that were performed on the biaxial MTS 809 axial / torque hydraulic testing system. Except for biaxial loading conditions, each test was controlled by a constant displacement/rotation ratio. The loading conditions with the applied crosshead speed of the experiment are provided in Fig. 3.

Taking into account the biaxial test, it requires a force control mode to provide a constant biaxiality ratio (λ_T) and phase proportionality. The two-biaxiality ratio was investigated. Firstly, the $\lambda_T = 1$, which means that the geometric stresses are the same. Then, the $\lambda_T = 0.5$, which provides 2 times greater geometrical shear stresses. Since it was important to maintain the constant increase in stress in each case, different torque/force velocities were applied for each biaxiality ratio. Strain gages and digital image correlation (Dantec dynamic Q300) were used to define the surface strains in the samples as presented in Fig. 4. They provided a reliable source for the deformation state of the sample under tensile, compression, and biaxial tests.

3. Numerical modeling

Section 3 includes the modeling process of the FW tube using the finite element method. In this section, the material model formulation that includes shear nonlinearity is described in detail. Furthermore, the applied boundary conditions and the mesh used are presented. The comparison of FE model with and without winding pattern (WP) is presented. A summary of the steps applied in this section is presented below.

1) Estimation of elastic properties based on Abolin'sh micromechanical approach,
2) Material model formulation (shear non-linearity effect),
3) FE model preparation (basic without and with winding pattern, BC, mesh),
4) Calibration of the model,
5) Validation of the model.

3.1. Modeling of nonlinear shear behavior

On the basis of mechanical experiments, the finite element method was applied for a semiempirical determination of the nonlinear shear model parameters proposed by Chang [13]. Elastic properties were calculated based on the micromechanics approach provided by Abolin'sh [18] for the fiber content equal to 55 % estimated on the basic of the scanning electron micrography pictures. Additionally, the hexagonal unit cell was created to compare the results of both approaches. The mechanical properties of the constituents were taken from Table 1. The estimated effective elastic properties are presented in Table 2. For the numerical simulation, the elastic properties calculated based on the Abolin'sh approach (Table 2) were taken into account.

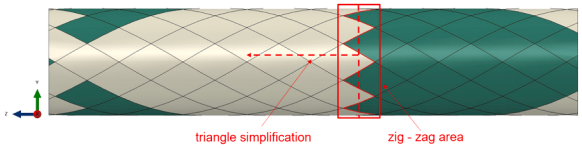

Fig. 5. FE modeling approaches—authors' concept including zigzag areas, and triangle concept sketched by dashed lines—possible simplification of material assignment.

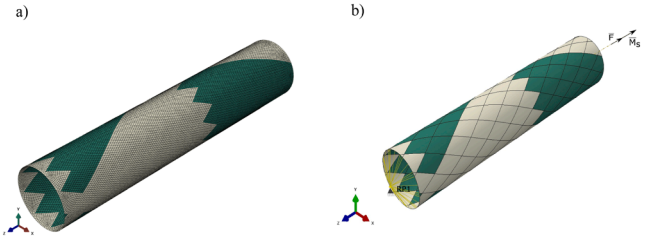

Fig. 6. a) Discrete model—material sections (various fiber orientations—different colors). b) boundary conditions applied to the FE model.

In addition to the elastic properties, the strength parameters presented in Table 3 along with the parameter that characterizes the nonlinearity of the material (α) were approximated using the FEM based on the experimental data of the conducted biaxial tests.

The softening effect of the stress-strain curve is caused by the accumulation of shear damage. This effect is multiplied by the complex geometry provided by the filament winding technology (interweaves). These aspects forces applying the material model that includes this effect. Several models are proposed in the literature [13,14,15,16,17], for this research, the one proposed by Chang was chosen. The nonlinear stress-strain relation in this model is represented by formula (2).

$$\gamma_{xy} = G_{xy}^{-1}\sigma_{xy} + \alpha\sigma_{xy}^{3} \tag{2}$$

where: G_{xy} is the (initial) ply shear modulus and nonlinearity is characterized by the factor α (2.44×10^{-6} MPa^{-3}).

The approximate range of the α parameter was estimated from the available literature [13,16]. The final value of α was empirically determined using the FEM based on the experimental results of the biaxial test.

The non-linear shear model implemented made the elastic properties dependent on the three variables implemented as field variables using the Abaqus subroutine USDFLD. Two of them (FV1, FV2) are binary variables that indicate the occurrence of failure, while the third (FV3) can have values in the range [0,1] indicating progressing shear damage. A wider description of the field variables and the theory behind them is presented below.

- *Field variable 1 (FV1)*—matrix tensile/compression failure Eqs. (3) and ((4)).
- *Field variable 2 (FV2)*—Fiber matrix shear failure (Eq. (5))
- *Field variable 3 (FV3)*—Material damage (shear nonlinearity) (Eq. (7))

The applied model takes into account the following failure mechanisms that are included in the FV:

- Matrix tensile cracking

$$e_m^2 = \left(\frac{\sigma_y}{Y_t}\right)^2 + \frac{\frac{2\sigma_{xy}^2}{G_{xy}} + 3\alpha\sigma_{xy}^4}{\frac{2S_c^2}{\sigma_{xy}} + 3\alpha S_c^4} \tag{3}$$

where, S_c – shear strength

- Matrix compressive failure

$$e_m^2 = \left(\frac{\sigma_y}{Y_c}\right)^2 + \frac{\frac{2\sigma_{xy}^2}{G_{xy}} + 3\alpha\sigma_{xy}^4}{\frac{2S_c^2}{\sigma_{xy}} + 3\alpha S_c^4} \tag{4}$$

$$\begin{cases} e_m^2 \geq 1 \rightarrow FV1 = 1 \\ e_m^2 < 1 \rightarrow FV1 = 0 \end{cases}$$

- Fiber-matrix shearing

$$e_{fs}^2 = \left(\frac{\sigma_x}{X_c}\right)^2 + \frac{\frac{2\sigma_{xy}^2}{G_{xy}} + 3\alpha\sigma_{xy}^4}{\frac{2S_c^2}{\sigma_{xy}} + 3\alpha S_c^4} \tag{5}$$

$$\begin{cases} e_{fs}^2 \geq 1 \rightarrow FV2 = 1 \\ e_{fs}^2 < 1 \rightarrow FV2 = 0 \end{cases}$$

- Fiber buckling—independent of the other stress components

$$e_b = -\frac{\sigma_x}{X_c} \tag{6}$$

Fiber buckling is a catastrophic failure mode and may subsequently follow fiber shearing due to shear stiffness degradation after shear fiber matrix failure. Therefore, after this failure occurs, it is assumed that the material cannot withstand any load.

- Damage parameter

$$d = \frac{3\alpha G_{xy}\left(\sigma_{xyi}^{(i)}\right)^2 - 2\alpha\left(\sigma_{xyi}^{(i)}\right)^3 \Big/ \gamma_{xy}^{(i)}}{1 + 3\alpha G_{xy}\left(\sigma_{xyi}^{(i)}\right)^2} \tag{7}$$

Finally, progressive damage is described by the relation presented in Eq. (8).

$$\sigma_{xy}^{(i+1)} = (1-d)G_{xy}\gamma_{xy}^{(i+1)} \tag{8}$$

3.2. Boundary conditions and mesh

Composite parts manufactured by the filament winding (FW) process are characterized by the presence of interweavings. This aspect influences the behavior of these parts in the elastic regime and during the initiation and propagation of damage. Taking into account the course of the FW process the external layer can have fibers running in $\alpha/-\alpha$ directions. The chosen pattern (based on the order of winding) can also influence the behavior of the model [19]. These aspects are usually taken into account by researchers by introducing triangular partitions of the geometry [20,21,22]. However, previous research conducted by our team shows that this simplification can lead to significant errors by omitting the so-called 'zig-zag' area and replacing it with a straight line as shown in Fig. 5.

The main problem with including a realistic geometry model that includes a 'zigzag' area is that such geometry is complex and cannot be easily produced manually. The solution to that is to create a model using scripting, which is possible in the Simulia Abaqus environment with

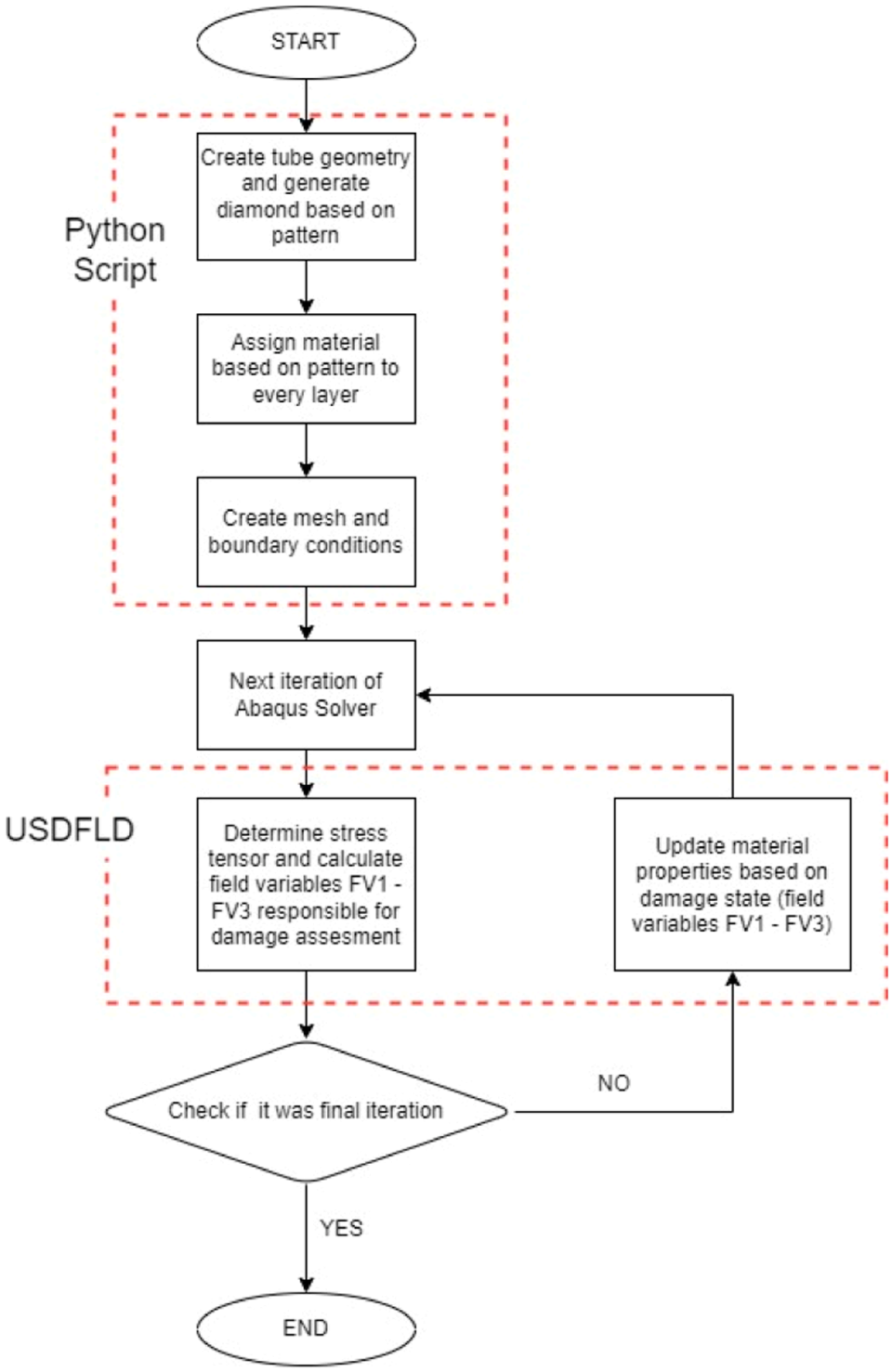

Fig. 7. Workflow of numerical simulations—model is generated with Python script due to the complexity of geometry and material distribution. During the solution of the model, the USDFLD subroutine written in Fortran is used to update the material properties due to the accumulation of progressive damage.

Python code. In this paper, we use the code developed previously in [23]. The effect of this approach (geometry partitions, material assignment, and mesh) is presented below in Fig. 6. The different angle orientation of the fibers is indicated by green and beige colors, respectively. Also, the zig-zag area is visible, and it will be visible later in the results section how its presence influences the results.

The applied mesh consists of 18,855 S4R elements.

A summary of the workflow used to process the numerical model is presented below in Fig. 7. The above-described approaches to geometry, material, and finite models are realized with the use of Python script (to generate geometry with 'diamond' partitions and assign material with respect to interweaving created in the filament winding process. Additionally, a material model is redefined after each iteration by introducing user-defined fields written in the Fortran subroutine USDFLD and assigning material properties based on calculated values of field variables.

To assess the effectiveness of the FE model with WP, a basic shell model with two $30/-30$ layers was created. Similar boundary condi-

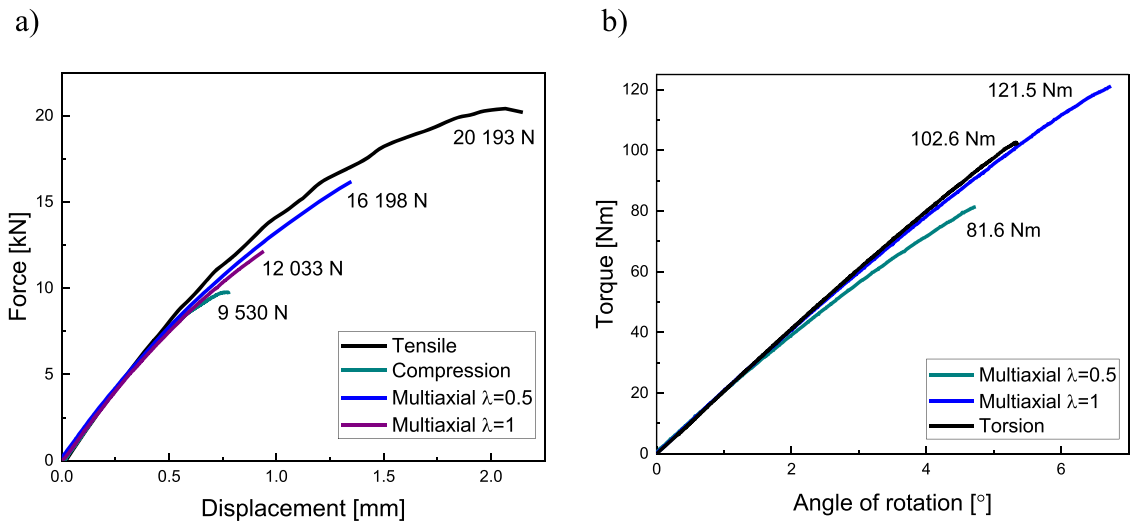

Fig. 8. a) Results of mechanical tests for tensile, compression and multiaxial loading conditions; b) Results of mechanical tests for torsional and multiaxial cases.

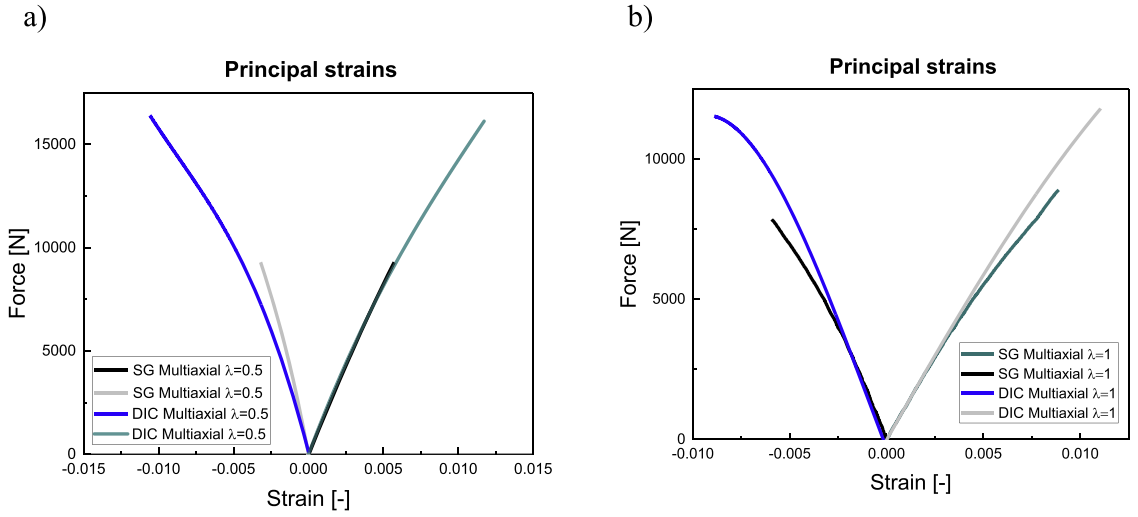

Fig. 9. a) Maximum principal stresses for multiaxial loading ($\lambda_T = 0.5$) obtained from strain gauges (SG) compared to those obtained from digital image correlation (DIC). b) maximum principal stresses for multiaxial loading ($\lambda_T = 1$) obtained from strain gauges compared to those obtained from digital image correlation.

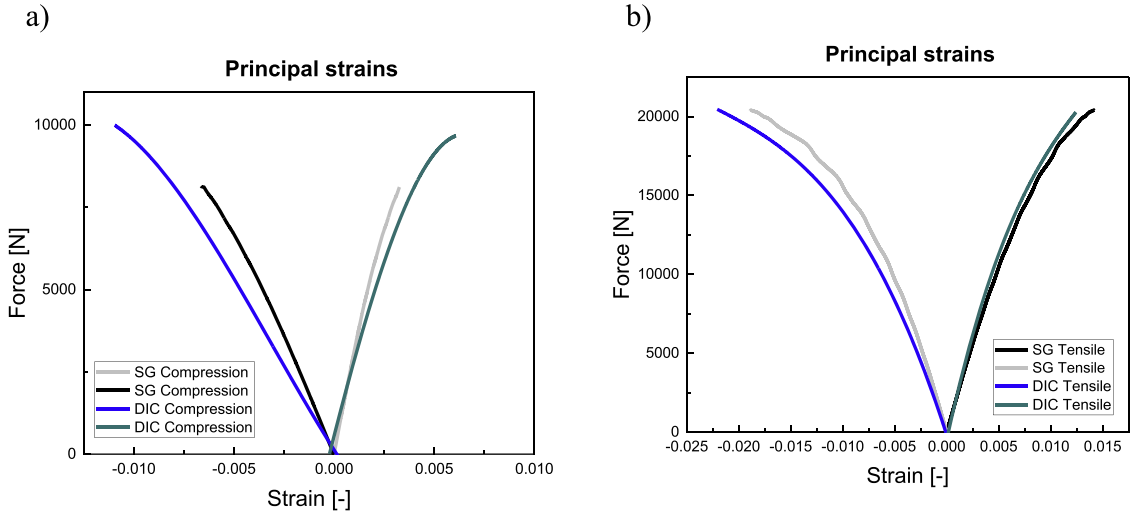

Fig. 10. a) Maximum principal stresses for compression obtained from strain gauges (SG) compared with those obtained from digital image correlation (DIC). b) maximum principal stresses for the tension obtained from the strain gauges compared with those obtained from digital image correlation.

Table 4
Comparison of results along with the relative error calculated at force 5 kN, where PS—principal strain.

Loading case	DIC	Strain gauge	Relative error at force 5 kN [%]
Max PS—tension [mm/mm]	0.012	0.013	2
Min PS—tension [mm/mm]	−0.22	−0.18	13
Max PS—multiaxial ($\lambda_T = 0.5$) [mm/mm]	0.011	0.005	3
Min PS—multiaxial ($\lambda_T = 0.5$) [mm/mm]	−0.010	−0.003	36
Max PS—multiaxial ($\lambda_T = 1$) [mm/mm]	0.010	0.008	2
Min PS—multiaxial ($\lambda_T = 1$) [mm/mm]	−0.008	−0.005	8
Max PS—compression [mm/mm]	0.005	0.003	26
Min PS—compression [mm/mm]	−0.010	−0.006	28

As presented in Table 4 relative error was calculated for the force equal to 5 kN. It shows the discrepancy in the strain results.

Table 5
Comparison of experimental results with FEA (with WP).

	Displacement at 8 Kn—experimental value	Displacement at 8 kN—FEA value	Relative error with respect to the experimental value at 8 kN
Multiaxial ($\lambda_T = 1$)	0.54 mm	0.54 mm	0 %
Multiaxial ($\lambda_T = 0.5$)	0.52 mm	0.54 mm	3.7 %
Tension	0.49 mm	0.52 mm	5.7 %
	Angle of rotation at 60 Nm—experimental value	Angle of rotation at 60 Nm—FEA value	Relative error with respect to experimental value at 60 Nm
Multiaxial ($\lambda_T = 0.5$)	3.23°	2.99°	8.0 %
Multiaxial ($\lambda_T = 1$)	3.03°	2.99°	1.3 %
Torsional	2.97°	2.93°	1.4 %

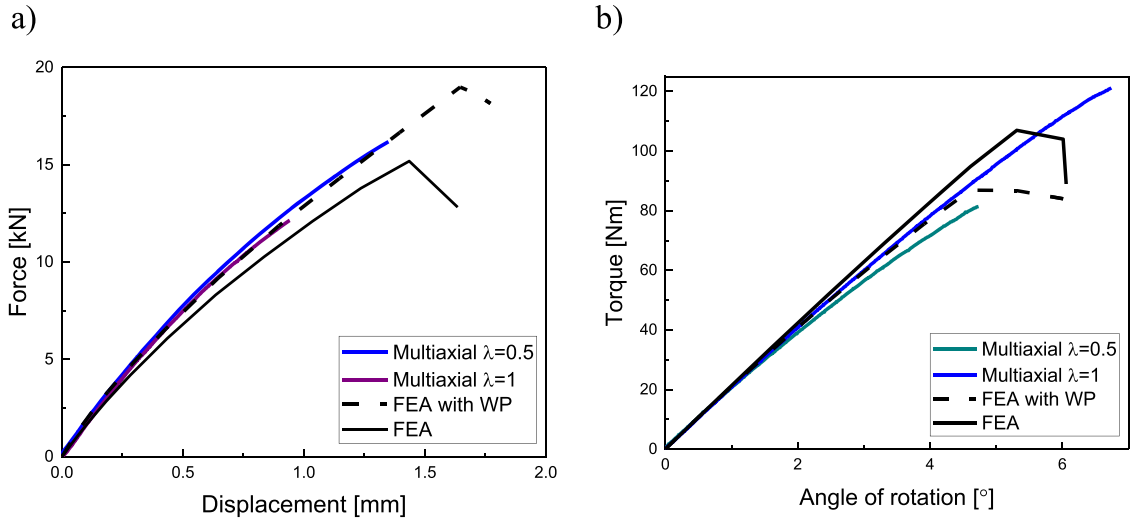

Fig. 11. Model validation a) comparison of multiaxial results for FEA (nonlinear shear model) and experiment. Presented experimental data was used for model calibration. b) Results of multiaxial torsional load in comparison for FEA and experiment (nonlinear shear model). Presented experimental data was used for model calibration.

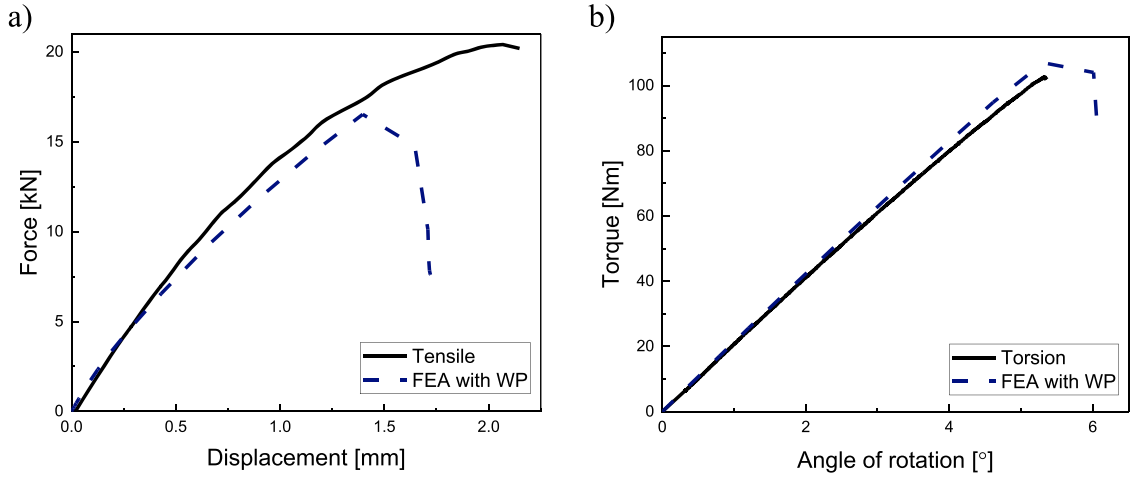

Fig. 12. Model validation a) comparison of the results of tensile load for FEA (based on the calibrated nonlinear shear model) and experiment. b) Torsional load results in comparison for FEA (based on the calibrated nonlinear shear model) and experiment.

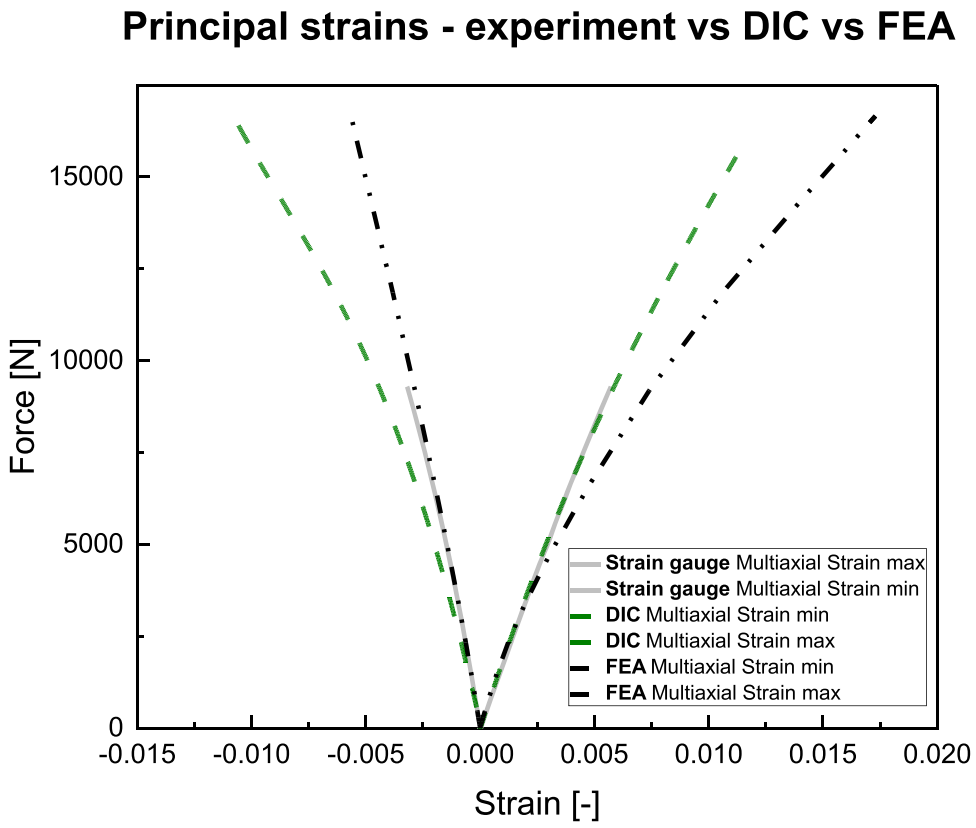

Fig. 13. Comparison of the principal strains for multiaxial $\lambda_T = 0.5$. The graph compares the values received from strain gauges, FEA and DIC.

tions are applied as for the model with WP. The mesh includes 6 300 S4R elements.

4. Results and discussions

Results and a discussion on the quasi-static experiments are presented in the first part of the section. Subsequently, the formulation and comparison of the strains obtained from strain gauge measurement and DIC is made. The last part summarizes the effectiveness of all the methods applied in this research.

4.1. Quasi-static experimental results

The results are divided into 2 graphs presenting the mechanical performance along the axial direction and rotational direction, Fig. 8.

As expected, the lower force value is obtained for compression -9530 N (131 MPa). On the other hand, the highest value of 20,193 N (279 MPa) was obtained for the tension. Moreover, a curve exhibits a slightly rough nature. This wavy shape might be caused by a small movement along the fibers (especially after debonding and delamination) that causes friction. Simultaneously, a very high tensile strength of the carbon fibers supports this phenomenon. Although the adhesion (matrix fiber) was partially damaged, the fibers could still have carried the load, causing friction and slipping that affected the shape of the curve. The torque load influences the final static strength as follows: 16,198 N (224 MPa for $\lambda_T = 0.5$) and 12,033 N (166 MPa for $\lambda_T = 1$). Considering the UTS for these two biaxialities, it can be stated that the axial force has a significant impact on the UTS.

4.2. Strain analysis - DIC vs. strain gauge

Furthermore, data from strain gauges are presented in Figs. 9 and 10. The rosette with 4 strain gauges was placed along the principal direction of the laminae (1—along fibers, 2—perpendicular to the direction of the fiber, and 12–45° from the first direction). It has allowed the delivery of the strain values for particular areas at the outer surface. These results were adopted for calibration and verification purposes.

The presented results show directly the non-linear elastic behavior of the specimen. This effect is known as shear softening, due to the high influence of shear stresses. This is even multiplied by the material architecture provided by the filament winding method. It gives the remark that commonly used material models (such as Hashin, Tsai-Hill, or Chamis) cannot be applied to this research case.

The deformation measurement using strain gauges was run for the duration of the static experimental campaign. Due to the large deformation of the samples, it was not possible to keep the strain gauges up to the strain at failure (maximum). The strain gauges deboned from the outer surface of the composite tube.

The principal strains obtained from the strain gauges and the DIC method are presented in Table 4.

4.3. Comparison of experimental results with FEA

This subsection presents a comparison of the force—displacement curves with the numerical results obtained from the FEA for the model with and without WP. The FE model with geometrical winding pattern (WP) and without is introduced and compared. Furthermore, the strain comparison is performed on the basis of the strain values from the strain gauges as a reference value for error calculations.

The results of the experiment were applied to calibrate and validate the material model in FEM. The non-linear shear model was calibrated based on multiaxial data according to Fig. 11. Experimental data allowed fitting the material non-linearity parameter α and estimating the strength parameters. The results of the calibrated FE model are presented in Fig. 11 for the discrete model with and without WP. As it is shown, the curve for FEA underestimates the axial stiffness of the tube,

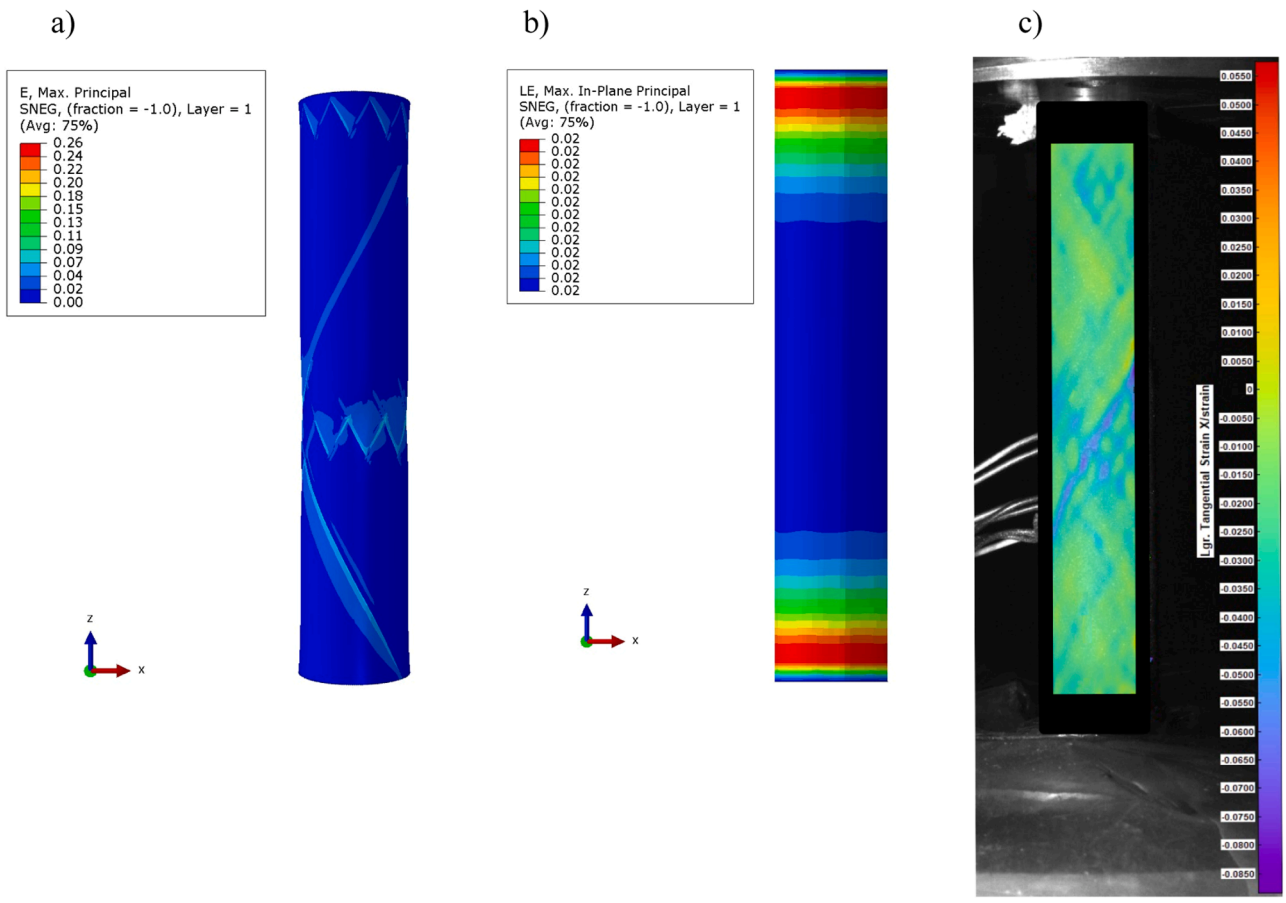

Fig. 14. Strain field comparison between a) FEA with WP, b) FEA without WP and c) DIC for multiaxial loading conditions.

per contra, the torsional stiffness is overestimated by the approach that does not include WP. In the next step of analysis, only the FE model with WP is applied.

The calibrated model was verified by predicting the mechanical response of the CFRP tube under tension and torsional loading. The prediction along with the experimental data is presented in Fig. 12. As is shown by the results in Fig. 11 some disagreement in the maximum forces is observed. It requires a more sophisticated procedure to precisely fit the strength parameters. Since the residual behavior is not within the scope of this investigation, the initial strength parameters obtained are applied.

The comparison of force and torque is presented in Table 5. Relative errors are calculated at the force level 8 kN, simultaneously, for the torsional load at the level of 60 Nm. The calculations are done with respect to the experimentally obtained values. The boundary load values are

The benchmark of the applied methods is shown in Fig. 13. As shown in terms of the minimum principal strains, the FE model better predicts the surface strain than the applied optical method (DIC). On the other hand, the maximum principal strain is more precisely predicted by digital image correlation. Due to the inhomogeneous strain distribution, it is difficult to take into account the same areas for each method. Only a small disagreement in the measured area led to a significant discrepancy in the results. Due to the high deformation of the sample surface, the strain gauges deboned and the value obtained from the strain gauges was inadequately lower and did not show the local maximum strain at failure.

Apart from the values comparison, strain and displacement fields for FEA and DIC are presented in Figs. 14 and 15. The strain and displacement fields presented by DIC show the effective deformation nature of the CFRP tube. On the other hand, the FEA with WP accurately predicts this deformation pattern. However, the FE model without WP exhibits an unrealistic strain pattern, which excludes the applicability of this approach in stress/strain analysis.

Because the investigated CFRP tube consists of only one FW layer, the zigzag area has a significant impact on the stress/strain distribution. In terms of the numerical model, the zigzag area is fixed at a certain tube length. However, as a result of manufacturing and sample preparation, the investigated tubes possess the zigzag area at various sample lengths. The strain pattern in Fig. 14 shows the general deformation manner; however, the local strain concentration can be shifted according to the positions of the zigzag areas, which is the critical area.

Concerning the deformation fields presented in Figs. 14 and 15, the effectiveness of the numerical analysis that includes WP can be highlighted. Both FE approaches present similar manner in the case of the total displacement; opposite case is given in strain fields; FE model without WP exhibits a uniform strain distribution along the sample circumference. This explains the discrepancy obtained in comparison to the experimental method. Moreover, the advantages of including the WP in the FE model are validated.

The relative error of the strain values obtained for the multiaxial loading conditions is presented in Table 6. It gives an error for the strains obtained from FEA, DIC in comparison to the maximum (0.0057) and minimum (−0.0032) strains obtained from the strain gauge rosette. As stated previously, the relative error for minimal principal strain is smaller in the case of the FEA, but the opposite situation occurs for the DIC method for maximum principal strain.

Remaining loading conditions exhibit different sensitivity to local strain concentration in zigzag area. It was not very well observed for the tension and compression. In terms of the torsional load, it was the weakest area of the tubular specimen and the area of final failure. In this case the local concentration along the zig-zag area was detrimental and

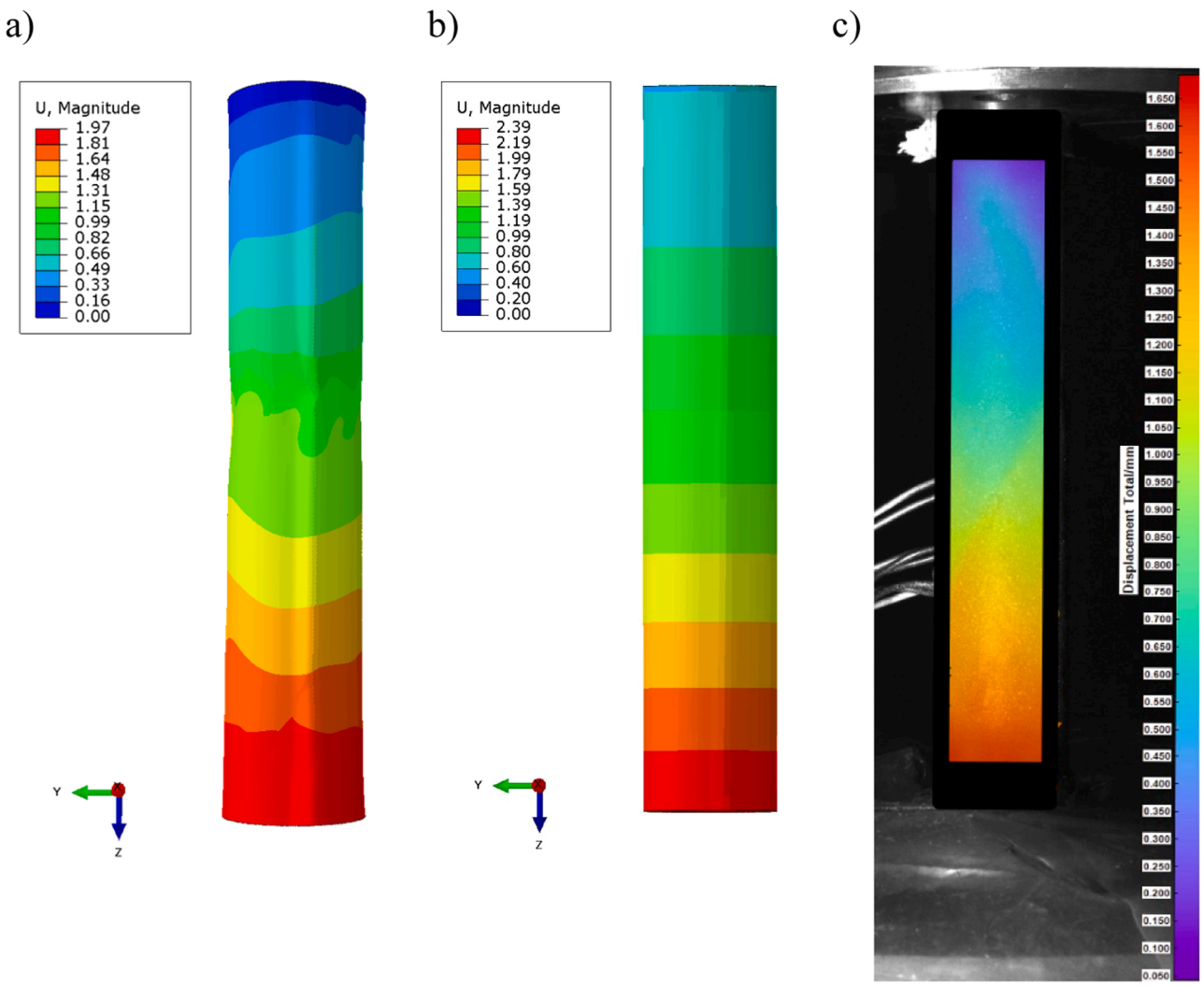

Fig. 15. Comparison of the total displacement field between a) FEA with WP b) FEA without WP and c) DIC for multiaxial loading conditions.

Table 6
Comparison of the relative error values for FEA and DIC with respect to the maximum and minimum strain obtained from the strain gauges.

	FEA	DIC
Relative error for positive principal strain (0.0057)	29.8 %	5.3 %
Relative error for negative principal strain (−0.0032)	12.5 %	34.4 %

caused the final failure, in contrast to the delamination failure caused by the strain concentration along the fiber tow in other loading cases.

The experimental campaign supported by strain gauges and the optical method allowed analysis of the strain field, calibration, and validation of the applied material model. The deformation observed via DIC allowed to assess this obtained from FEA. The major deformation has been placed along the fiber tow and around the zigzag area, which is confirmed by the DIC and FEA. It suggests a good correlation and model calibration with real conditions.

5. Conclusions

The presented work analyzes the mechanical performance of CFRP thin-walled structures under various loads, such as tension, compression, torsion, and their combination. The results of the experiment exhibit the nonlinear stress-strain behavior of the material. This behavior was reflected by using the numerical method. A non-linear shear model was capable of predicting the mechanical behavior of the investigated structures.

On the basis of the conducted research, the following conclusions can be drawn.

- Due to the inhomogeneity of the strain distribution in the FW tube, the analysis of stress/strain requires a comprehensive experimental procedure combined with additional methods, such as strain gauges or optical measurements.
- The comprehensive experimental procedure allows for calibrating the proper material model and implementing it into the FE model. Proper validated material model allows sophisticated stress analysis of the FW tube.
- DIC is a useful method to determine surface strain in thin-walled CFRP tubes. This optical method can be validated by using strain gauge measurement. However, strain gauges require a very precise preparation of the surface and bonding procedure. Due to the relatively high deformation, the strain gauges can debone from the surface. It complicates the problem of reaching the failure strain.
- A complex numerical model of a multiaxial loaded CFRP tube was created and analyzed. A Python script was used to prepare the precise geometry of the tube. It takes into account the FW pattern and the zigzag areas that are crucial in the stress/strain analysis. Proper geometrical reflection of the material architecture allows for better

stress-strain prediction. The effectiveness of the approach was validated by comparing it with the FE model that does not include WP. This approach does not provide adequate strain fields. Simultaneously, it over- and underestimates the stress-strain behavior.

- By introducing the Fortran user subroutine USDFLD, it was possible to incorporate the model including the shear non-linearity proposed by Chang. During the research, good compliance was found between the numerical models derived in this way and the experiments carried out. Thus, the presented approach can be successfully applied to similar problems. The calibrated non-linear shear model allowed for a precise prediction of the CFRP tubes under various loading conditions. It is proved by experiment. Furthermore, the deformation fields provided by FEA exhibit a manner similar to the real ones captured by DIC.
- The comparison of the methods shows that FEA gives more accurate results for the minimum principal strains than the applied optical method (DIC). On the other hand, the maximum principal strain is more precisely predicted by digital image correlation. In terms of FEA, the area and method of stress/strain assessment play a crucial role and define the error margin.
- Micromechanical approaches that include homogenization using unit cells or those based on compliance and stiffness tensors such as Rule of Mixture or Abolin'sh provide reliable elastic properties of the material. As it is presented, the results are accurate; only in the transverse direction is a disagreement noticeable. However, these approaches require data for constituents, which may be taken either from the literature or by experiment. It should be noted that they do not provide the strength parameters for the material.
- Concerning the observed failure of the thin-walled CFRP tube, it should be noted that the stress concentration is clearly visible along the fiber tow and zigzag areas. For torsional loading, the final failure occurred in a zigzag area. In terms of the other loading cases (tension, compression, bi-axial) the final failure was caused by the delamination along the fiber tows.

CRediT authorship contribution statement

Szymon Duda: Conceptualization, Methodology, Validation, Formal analysis, Investigation, Resources, Data curation, Writing – original draft, Writing – review & editing, Visualization, Project administration, Funding acquisition. **Michał Smolnicki:** Software, Writing – original draft, Writing – review & editing. **Paweł Stabla:** Validation, Data curation. **Paweł Zielonka:** Validation, Investigation, Data curation. **Tomasz Osiecki:** Resources, Visualization. **Chao Gao:** Formal analysis, Writing – review & editing, Supervision. **Grzegorz Lesiuk:** Methodology, Formal analysis, Supervision, Funding acquisition, Resources.

Declaration of Competing Interest

The authors declare the following financial interests/personal relationships which may be considered as potential competing interests:

Szymon Duda reports financial support was provided by National Science Centre Poland.

Data availability

Data will be made available on request.

Acknowledgments

This research was partially or fully funded by the Polish National Science Center Grant no. 2021/41/N/ST8/03365. Calculations have been carried out using resources provided by Wroclaw Centre for Networking and Supercomputing (http://wcss.pl), Grant no. 531.

References

[1] J. Weng, T. Meng, W. Wen, S. Weng, Multiaxial fatigue life prediction of composite laminates, Chin. J. Aeronaut. (2020), https://doi.org/10.1016/j.cja.2020.06.016.
[2] D. Qi, G. Cheng, Failure analysis of fiber-reinforced composites under multiaxial cyclic stress, Polym. Compos. 29 (8) (2008) 922–931, https://doi.org/10.1002/pc.20419.
[3] M. Quaresimin, 2.13 multiaxial fatigue of composites: experimental evidences and life prediction methodology. Comprehensive Composite Materials II, Elsevier, 2018, pp. 249–274, https://doi.org/10.1016/B978-0-12-803581-8.09915-X.
[4] M. Quaresimin, 50th anniversary article: multiaxial fatigue testing of composites: from the pioneers to future directions, Strain 51 (1) (2015) 16–29, https://doi.org/10.1111/str.12124.
[5] R. Olsson, A survey of test methods for multiaxial and out-of-plane strength of composite laminates, Compos. Sci. Technol. 71 (6) (2011) 773–783, https://doi.org/10.1016/j.compscitech.2011.01.022. Elsevier.
[6] M. Quaresimin, P.A. Carraro, Damage initiation and evolution in glass/epoxy tubes subjected to combined tension-torsion fatigue loading, Int. J. Fatigue 63 (2014) 25–35, https://doi.org/10.1016/j.ijfatigue.2014.01.002.
[7] V.V. Vasiliev, E.V. Morozov, Advanced Mechanics of Composite Materials and Structural Elements, Elsevier Science, 2013.
[8] E.A.W. de Menezes, T.V. Lisbôa, J.H.S. Almeida, A. Spickenheuer, S.C. Amico, R. J. Marczak, On the winding pattern influence for filament wound cylinders under axial compression, torsion, and internal pressure loads, Thin-Walled Struct. 191 (2023), 111041, https://doi.org/10.1016/j.tws.2023.111041.
[9] T.V. Lisbôa, J.H.S. Almeida, I.H. Dalibor, A. Spickenheuer, R.J. Marczak, S. C. Amico, The role of winding pattern on filament wound composite cylinders under radial compression, Polym. Compos. 41 (6) (2020) 2446–2454, https://doi.org/10.1002/pc.25548.
[10] C.B. Azevedo, J.H.S. Almeida, H.F. Flores, F. Eggers, S.C. Amico, Influence of mosaic pattern on hygrothermally-aged filament wound composite cylinders under axial compression, J. Compos. Mater. 54 (19) (2020) 2651–2659, https://doi.org/10.1177/0021998319899144/ASSET/IMAGES/LARGE/10.1177_0021998319899144-FIG7.JPEG.
[11] E.V. Morozov, The effect of filament-winding mosaic patterns on the strength of thin-walled composite shells, Compos. Struct. 76 (1–2) (2006) 123–129, https://doi.org/10.1016/J.COMPSTRUCT.2006.06.018.
[12] M. Sayem Uddin, E.V. Morozov, K. Shankar, The effect of filament winding mosaic pattern on the stress state of filament wound composite flywheel disk, Compos. Struct. 107 (1) (2014) 260–275, https://doi.org/10.1016/J.COMPSTRUCT.2013.07.004.
[13] F.K. Chang and L.B. Lessard, "Damage tolerance of laminated composites containing an open hole and subjected to compressive loadings: part I—Analysis,", vol. 25, no. 1, pp. 2–43, 1991, 10.1177/002199839102500101.
[14] W. Van Paepegem, I. De Baere, J. Degrieck, Modelling the nonlinear shear stress–strain response of glass fibre-reinforced composites. Part II: model development and finite element simulations, Compos. Sci. Technol. 66 (10) (2006) 1465–1478, https://doi.org/10.1016/J.COMPSCITECH.2005.04.018.
[15] Y. He, A. Makeev, B. Shonkwiler, Characterization of nonlinear shear properties for composite materials using digital image correlation and finite element analysis, Compos. Sci. Technol. 73 (1) (2012) 64–71, https://doi.org/10.1016/J.COMPSCITECH.2012.09.010.
[16] B. Fedulov, A. Fedorenko, A. Safonov, E. Lomakin, Nonlinear shear behavior and failure of composite materials under plane stress conditions, Acta Mech. 228 (6) (2017) 2033–2040, https://doi.org/10.1007/S00707-017-1817-4/METRICS.
[17] C.N. O'Brien, A.E. Zaghi, Modelling the nonlinear shear stress-strain response of composites with metal and non-metal reinforcement, Compos. B Eng. 221 (2021), 109009, https://doi.org/10.1016/J.COMPOSITESB.2021.109009.
[18] D.S. Abolin'sh, Compliance tensor for an elastic material reinforced in one direction, Polym. Mech. 1 (4) (1965) 28–32, https://doi.org/10.1007/BF00858888/METRICS.
[19] P. Stabla, M. Lubecki, M. Smolnicki, The effect of mosaic pattern and winding angle on radially compressed filament-wound CFRP composite tubes, Compos. Struct. 292 (2022), 115644, https://doi.org/10.1016/J.COMPSTRUCT.2022.115644.
[20] M.K. Akhtar, W.A. Qureshi, R. Jamshed, M. Raza, Analytical modeling and numerical analysis of the effect of mosaic patterns on composite pressure vessels with dome, J. Reinf. Plast. Compos. 40 (17–18) (2021) 621–631, https://doi.org/10.1177/0731684421994326.
[21] C. Baierle de Azevedo, F. Eggers, H. Feitosa Flores, S. Amico, J.H. Almeida Júnior, On the importance of the filament winding pattern of composite cylinders in axial compression: damage and buckling analyses, in: *Proceedings of the 7th International Symposium on Solid Mechanics*, ABCM, 2019, https://doi.org/10.26678/ABCM.MECSOL2019.MSL19-0177.
[22] T.V. Lisbôa, J.H.S. Almeida Jr., A. Spickenheuer, M. Stommel, S.C. Amico, R. J. Marczak, FEM updating for damage modeling of composite cylinders under radial compression considering the winding pattern, Thin-Walled Struct. 173 (2022), 108954, https://doi.org/10.1016/j.tws.2022.108954.
[23] P. Stabla, M. Smolnicki, and W. Błażejewski, "The numerical approach to mosaic patterns in filament-wound composite pipes," *Appl. Compos. Mater.*, 123AD, doi: 10.1007/s10443-020-09861-z.